Int. J. Heat Mass Transfer. Vol. 30, No. 8, pp. 1663–1672, 1987
Printed in Great Britain

0017–9310/87 $3.00 + 0.00

Wall–particles heat transfer in rotating heat exchangers

P. LYBAERT
Faculté Polytechnique de Mons, Laboratoire de Thermique, rue de l'Epargne, 56, B-7000 Mons, Belgium

(*Received* 4 *October* 1986 *and in final form* 26 *January* 1987)

Abstract—The wall–particles heat transfer coefficient has been measured in small-scale rotary drum heat exchangers. Experiments have been conducted with nine granular materials of different nature, with particle diameters ranging from 194 μm to 4 mm. The effects of rotational speed (1–40 rev min^{-1}), filling degree (4–17%) and drum diameter (0.25 and 0.485 m) have been investigated. The experimental data have been correlated by a semi-empirical relationship, that includes a contact resistance at the wall, the heat capacity of the particles immediately adjacent to the wall and the heat penetration resistance of the bulk of the particle bed. The contact resistance is shown to be due to the roughness of the particles. A mean roughness height of 12 μm provides a good fit to the measured coefficients.

INTRODUCTION

ROTARY drum heat exchangers are widely used in industry for the heat-treatment of granular solids. When the heating medium is a gas, direct contact equipment is generally preferred. When it is not so—liquid, condensing steam, . . .—or when the direct contact may be detrimental to the material, indirect heat transfer is necessary: heat is then transferred to the particles through a wall. In this study, we will restrict our interest to this latter case, particularly when the cylinder wall forms the heat transfer surface.

Few publications have been devoted specifically to the wall–particles heat transfer in rotary drums and experimental values of heat transfer coefficients are rather sparse.

The first approach is due to Wes *et al.* [1]. These authors have measured contact heat transfer coefficients between carbohydrate particles and a cylinder externally heated by steam. The drum diameter was 0.6 m and nine longitudinal strips were welded on the inner wall. For charges of starch and dextrine, with particle diameters between 15 and 100 μm, and for rotational speeds lower than 7 rev min^{-1} the measured coefficient was found to vary with the square root of the speed.

Lehmberg *et al.* [2] observed the transverse movement and mixing of sand and sodium carbonate particles in a small cylinder. They measured the time of radial dispersion of a small batch of coloured particles within the load. From these measurements, they concluded that the intensity of radial mixing is fairly high. In addition, they determined the transfer coefficient between the material and the wall of a small water-cooled cylinder. The wall of the cylinder was smooth. The drum diameter was 0.25 m and had a length of 0.6 m. They used batches of silica sand, with mean particle diameters of 157, 323, 794 and 1038 μm, and sodium carbonate particles with a mean granulometry of 137 μm. The time of contact between the particles and the wall ranged from 0.6 to 40 s. The measured values increase when the contact time decreases. At low values of the contact time, the transfer coefficient tends to an asymptotic value that depends on the particle diameter: higher limiting values are obtained with smaller particles.

To account for their experimental results, Lehmberg *et al.* used a penetration model, the particle bed being considered as a semi-infinite homogeneous body whose physical properties are equal to the apparent properties of the material. The transfer limitation at high rotational speeds was explained by the existence of a gas film between the particles and the wall. A contact resistance, whose value depends on the particles dimension, was associated to this film. By adjusting the value of the contact resistance, a good fitting of the measured coefficients could be obtained.

The aim of the present work is to extend the scope of the former studies by a systematic experimental investigation of the effect of the different parameters influencing the contact heat transfer between a granular material and the wall of an indirect rotating exchanger. New heat transfer correlations, taking these effects into account, will be provided.

MEASUREMENTS OF WALL–PARTICLES HEAT TRANSFER COEFFICIENTS

Experimental methods

The heat transfer coefficients are determined in a horizontal batch fed cylinder, 0.6 m long. This cylinder is heated externally by an electrical resistance and insulated by a layer of mineral wool.

The temperature of the wall is measured by six thermocouples:

(a) four of them, placed 90° apart and connected in

NOMENCLATURE

a	surface coverage factor
a_0	apparent thermal diffusivity of the granular material
c_0	specific heat of the granular material
c_w	specific heat of the drum wall
c_s	particle specific heat
C_c	contact heat capacity
D_p	particle diameter
D_t	drum diameter
Fo	Fourier number, $a_0\tau/D_p^2$
Fr	Froude number of the cylinder, $\omega^2 D_t/2g$
g	gravitational acceleration
J	filling degree
K	instantaneous heat transfer coefficient
$\bar{K}$	time-mean heat transfer coefficient
K_c	contact heat transfer coefficient
K_w	wall-to-bed heat transfer coefficient
m	mass of material introduced in the drum
m_w	mass of the cylinder wall
N	rotational speed [rev min^{-1}]
$\overline{Nu}$	time-mean Nusselt number, $\bar{K}D_p/\lambda_g$
Nu_c	contact Nusselt number, $K_c D_p/\lambda_g$
$\overline{Nu}_0$	time-mean Nusselt number, relative to homogeneous solid, equation (23)
p_1, p_2	reciprocal time constants in equation (7)
S	surface area
S_w	particles–drum contact area
t	temperature
t_a	ambient temperature
t_m	mean temperature of the material
t_{m0}	initial value of t_m
t_w	temperature of the wall
t_{w0}	initial value of t_w
x	distance from the surface.

Greek symbols

α	heat loss coefficient
δ	distance between the wall and the first layer of particles
ε_0	void fraction of the granular material
λ_g	thermal conductivity of the gas
λ_0	apparent thermal conductivity of the granular material
ρ_0	bulk density of the material
ρ_s	particle density
τ	time
τ_c	time of particle contact with the wall
τ_m	material time constant in equation (7)
τ_w	wall time constant in equation (7)
ϕ	heat flux
Φ	heat flow
ψ	filling angle
ω	angular speed.

series, measure the wall temperature at the midlength of the drum;

(b) the two others, placed at respectively 25 and 75% of the length, are used to estimate the longitudinal temperature gradient in the wall.

The heat transfer coefficient is determined from the transient evolution of the wall temperature during the heating of a batch of particles: the empty rotating drum is heated by application of a constant power Φ_0 and reaches, after a while, a steady-state temperature t_{w0}. At this time, a fixed quantity of material, at ambient temperature, is introduced into the drum. The heating power remaining unchanged, this operation yields a wall temperature variation which essentially depends on the wall–charge heat transfer rate.

A typical experimental curve is represented in Fig. 1.

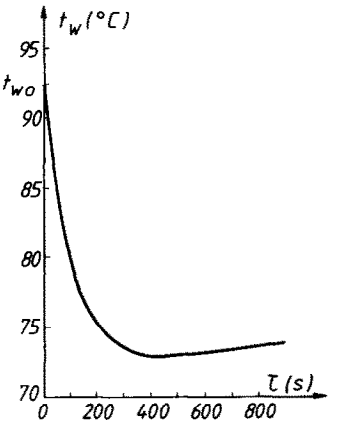

FIG. 1. Measurement of the heat transfer coefficient. Typical evolution of the wall temperature.

The determination of the heat transfer coefficient from this curve is obtained by identification with a mathematical model.

A lumped parameter model is adopted, according to the following assumptions:

(a) the axial and radial temperature gradients in the wall are neglected, the wall temperature is assumed uniform;

(b) the load temperature is uniform;

(c) the heat transfer coefficient between the wall and the material is constant during the test;

(d) the heat loss coefficient between the wall and the ambiance is constant.

With these assumptions, the transient heat balance of the system is described by

$$mc_0 \frac{dt_m}{d\tau} + m_w c_w \frac{dt_w}{d\tau} = \Phi_0 - \alpha(t_w - t_a). \qquad (1)$$

Noting that

$$\Phi_0 = \alpha(t_{w0} - t_a) \tag{2}$$

equation (1) can be written as

$$mc_0 \frac{dt_m}{d\tau} + m_w c_w \frac{dt_w}{d\tau} = \alpha(t_{w0} - t_w). \tag{3}$$

On the other hand, the balance for the material is given by

$$mc_0 \frac{dt_m}{d\tau} = K_w S_w (t_w - t_m). \tag{4}$$

The following initial conditions hold for t_w and t_m :

$$t_w(\tau = 0) = t_{w0} \tag{5}$$

$$t_m(\tau = 0) = t_{m0}. \tag{6}$$

Equations (3) and (4) are solved by applying the Laplace transformation to both equations. The transformed equations are then solved with respect to the transform of t_w. Using the inverse transformation, the following expression is obtained for the time variation of the wall temperature:

$$\frac{t_w - t_{w0}}{t_{w0} - t_{m0}} = -\frac{mc_0}{m_w c_w \tau_m (p_1 - p_2)} [\exp(p_1\tau) - \exp(p_2\tau)]$$

$$p_1 \text{ and } p_2 = -\frac{m_w c_w + mc_0}{2m_w c_w \tau_m}$$

$$\times \left[1 + \frac{\tau_m}{\tau_w} \mp \sqrt{\left(\left(1 + \frac{\tau_m}{\tau_w}\right)^2 - \frac{4m_w c_w \tau_m}{(m_w c_w + mc_0)\tau_w}\right)}\right] \tag{7}$$

with

$$\tau_m = \frac{mc_0}{K_w S_w}, \quad \tau_w = \frac{m_w c_w + mc_0}{\alpha}.$$

The wall heat capacity $m_w c_w$ and the heat loss coefficient α, which in principle should be directly calculated from the data of the problem, are actually not precisely known. Therefore, they are considered as unknown parameters and evaluated, together with the product $K_w S_w$, by fitting the measured values of the wall temperature with relation (7). A statistical analysis of the set of all the $m_w c_w$ and α values obtained allows the validity of the experimental method to be checked [3].

The values of S_w, the contact areas of the material on the wall are determined from separate experiments. As to the apparent properties of the different materials used for the tests, they are measured by standard methods: the thermal conductivity by the hot-wire method and the heat capacity by a calorimetric method.

Table 1. Experimental conditions

Cylinder geometry:	
wall fitted out with eight longitudinal strips	
	$D_t = 0.25$ m
	$D_t = 0.485$ m
smooth wall	$D_t = 0.25$ m
Rotational speed:	1–40 rev min^{-1}
Filling degree J:	5–17%
Granular materials, particle diameter D_p	
glass beads:	500, 2000, 4000 μm
silica sands:	194, 343, 709, 924 μm
steel shots:	400, 2200 μm
Wall temperature t_w:	70–90°C
Material temperature t_m:	20–80°C

Experimental conditions

The experimental conditions are summarized in Table 1.

Two cylinders of different diameters were used: 0.25 and 0.485 m. For most of the tests, in order to avoid the sliding of the load on the wall, the latter was provided with eight longitudinal strips; these were made of low conducting material (Pical) in order not to take part in the heat transmission. Their relative height was around 3% of the inner diameter. One series of tests was performed in a smooth wall cylinder of 0.25 m diameter.

Nine granular materials of different nature (glass, silica sand and steel) and granulometry (194 μm–4 mm) were tested. Their physical properties are given in Table 2.

Analysis of the experimental results

The enumeration of all the variables which might *a priori* influence the heat transfer from the wall to the particles leads to the following relation for K_w:

$$K_w = F(\omega, D_p, \text{material nature}, J, D_t, \text{cylinder geometry}).$$

We will now discuss the effects of these different variables as they appear from our experimental results. Starting with the tests carried out in the strip-fitted drums, we can make the following comments.

The effect of the rotational speed exhibits the typical aspect shown on Fig. 2. For materials of the same nature, the heat transfer coefficient depends on the speed and the particle diameter:

(a) the coefficient increases with the speed, the variation being greater for smaller diameters and smaller speeds;

(b) the coefficient increases when the granulometry goes down, this effect being stronger at higher speeds;

(c) for low speeds, the coefficient is not dependent on the particle dimensions and depends on the nature of the material; at high speeds, the coefficient depends markedly on the diameter, with the material nature having but a secondary influence;

(d) orders of magnitude for the coefficients measured in the smallest drum are as follows:

Table 2. Physical properties of the tested materials

Material	Glass			Silica sand				Steel	
D_p (μm)	500	2000	4000	194	343	709	924	400	2200
ρ_0 (kg m^{-3})	1653	1576	1518	1485	1530	1590	1475	4160	4620
ρ_s (kg m^{-3})	2660	2515	2500	2640	2640	2635	2645	7800	7800
ε_0	0.379	0.373	0.393	0.438	0.420	0.397	0.442	0.467	0.408
c_0 (J kg^{-1} °C^{-1})	734	836	836	848	848	848	848	451	451
λ_0 (W m^{-1} °C^{-1})	0.196	0.222	0.258	0.278	0.281	0.305	0.257	0.345	0.442
$a_0 \times 10^7$ (m^2 s^{-1})	1.615	1.685	2.033	2.208	2.166	2.262	2.055	1.836	2.121

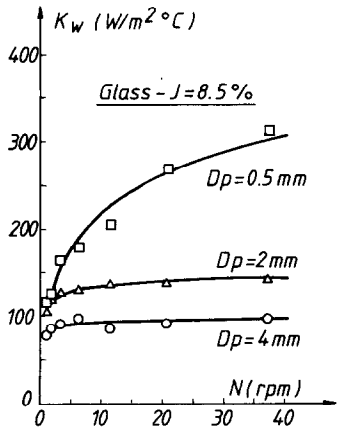

FIG. 2. Effect of the rotational speed on the heat transfer coefficient.

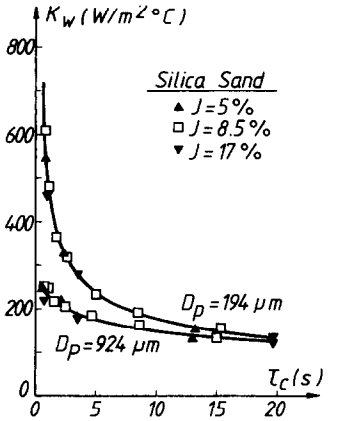

FIG. 3. Effect of the filling degree on the heat transfer coefficient.

$N = 1$ rev min^{-1}: glass beads 100 W m^{-2} °C^{-1}

silica sands 120 W m^{-2} °C^{-1}

steel shots 130 W m^{-2} °C^{-1}

$N = 40$ rev min^{-1}: from 100 W m^{-2} °C^{-1} (glass beads, 4 mm) to 600 W m^{-2} °C^{-1} (sand, 194 μm).

The effect of the filling degree J has been investigated in the small drum. For a given rotational speed, an increase of the filling degree leads to a decrease of the transfer coefficient.

This effect is entirely due to the variation of the contact time of the particles at the wall, which is related to the filling angle ψ, in no-sliding conditions, by

$$\tau_c = \frac{\psi}{\omega}. \tag{8}$$

When, indeed, K_w is plotted against τ_c, the values obtained for different filling degrees fall along a unique curve (Fig. 3).

The effect of the cylinder diameter has been investigated with six materials (sand, 194 and 924 μm; glass beads, 2 and 4 mm; steel shot, 400 μm and 2.2 mm). The coefficients measured for steel shots are plotted in Fig. 4: at a given contact time, the differences between the K_w values obtained with the two cylinders are within the experimental errors. This has been observed for all tested materials.

As to the coefficients measured in the smooth wall

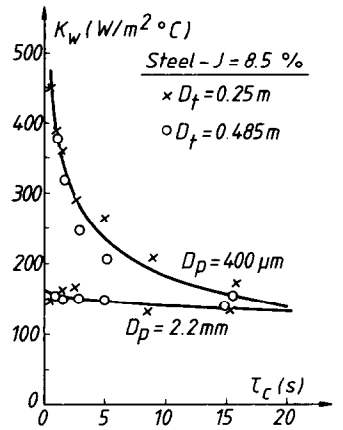

FIG. 4. Effect of the drum diameter on the heat transfer coefficient.

cylinder, they are smaller—all other conditions being equal—than those determined in the drum fitted out with strips (Fig. 5). The differences between the two series of tests increase with rotational speed. These differences seem to be due to the sliding of the load on the wall: the rotational speed of the particles in the vicinity of the wall is smaller than the speed of the cylinder. This sliding is confirmed by a visual observation of the load: the circulation of particles is less intense when the wall is smooth.

The visual inspection also indicates that the movement of the load is markedly affected by the end walls of the drum in this case. This effect is peculiar to batch fed cylinders and is not expected to occur in industrial

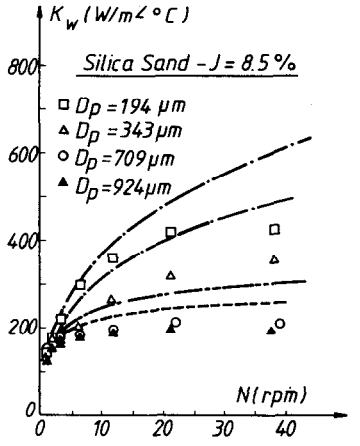

FIG. 5. Effect of the cylinder geometry on the heat transfer coefficient: point values, smooth wall; lines, wall fitted out with eight longitudinal strips.

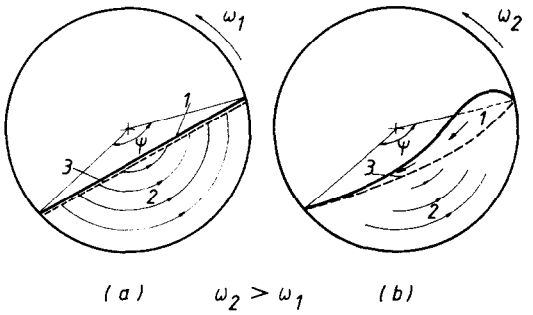

FIG. 6. Transverse motion of the load in a rotating cylinder: (1) cascade zone; (2) fixed bed zone; (3) rupture surface.

equipment. Therefore, the measurements performed in the smooth wall drum will not be considered further in this paper.

CORRELATION OF THE EXPERIMENTAL HEAT TRANSFER COEFFICIENTS

Mechanisms of heat transfer—penetration model

The heat transfer by contact between the load and the wall depends on the transverse motion of the material. This motion has been described by several authors [2, 4–8]. It is primarily influenced by the gravitational and centrifugal forces acting on the load and is therefore related to the value of a Froude number defined as

$$Fr = \frac{\omega^2 D_t}{2g}. \tag{9}$$

For Froude numbers encountered in industrial practice, i.e. less than 0.25, the motion pattern is of the 'cascading' type.

(1) At low speeds of rotation (Fig. 6(a)), the load is divided into two zones, separated by a rupture surface. In the first zone the material behaves like a fixed bed that follows the motion of the wall: the particles are fixed relative to their neighbours, their paths being circular arcs concentric to the cylinder. On reaching the rupture surface, the particles roll down the surface of the bed in a thin layer ('cascade' zone).

(2) With increasing speed (Fig. 6(b)), the flowrate of particles in the cascade and the thickness of this zone increase. As a result of the centrifugal forces, the rupture surface becomes curved and the surface of contact between the load and the wall increases.

If the friction forces at the wall are insufficient, some sliding of the particles is observed near the wall [6, 7]. With very low friction coefficients, the particles do not circulate at all ('sliding'). This relative motion between the particles and the wall can be avoided by attaching longitudinal strips to the wall.

According to this picture, the heat transfer is due to the circulation of the particles between the wall and the cascade zone. Two basic mechanisms are involved:

(a) the heating of the particles during their stay in the vicinity of the wall;

(b) the mixing of hot and cold particles in the cascade zone.

This heat transfer mechanism can be best described by a penetration model. Such models have been widely used to describe heat transfer in agitated [9] and fluidized beds [10–15]. Wes *et al.* [1] and Lehmberg *et al.* [2] applied this model to account for their results in rotating cylinders.

The model relates the heat transfer at the wall to the periodical replacement of 'packets' of particles. These packets, at uniform initial temperature t, come in contact with the wall, exchange heat by conduction during their residence time at the wall and then return into the load. The heat penetration depth is assumed to be smaller than the dimensions of the packets so that they can be considered as semi-infinite bodies.

The instantaneous heat flux between the wall and a single packet is related to the age and the initial temperature of the packet by

$$\phi(\tau) = K(\tau)(t_w - t). \tag{10}$$

By integration of this expression, the heat flow transferred by the wall is obtained

$$\Phi = \int_{S_w} K(\tau)(t_w - t)\, \mathrm{d}S(\tau, t). \tag{11}$$

In integral (11), $\mathrm{d}S(\tau, t)$ is the wall area covered by packets the ages of which are comprised between τ and $\tau + \mathrm{d}\tau$ and initial temperatures between t and $t + \mathrm{d}t$.

To estimate integral (11), the age and initial temperature distributions have to be known.

In a rotating exchanger, each particle at the wall has the same contact time. If the load does not slide on the wall, this time is given by equation (8) and it becomes

$$\tau_c = (\psi/\omega) \cdot F(sliding) \quad \text{with} \quad F(sliding) > 1 \tag{12}$$

if some sliding takes place. Consequently, the residence time distribution of the packets at the wall is uniform.

The distribution of the initial temperatures depends

on the intensity of mixing of hot and cold particles in the cascade. This phenomenon is very complicated and the distribution cannot be calculated theoretically. We will assume that thermal mixing in the cascade zone is complete, this means that the distribution of the initial temperatures of the packets is identical to the one of the temperatures inside the load. Accordingly, the mean initial temperature of the packets is equal to the mean temperature of the material t_m.

This assumption has been demonstrated to be appropriate at low speeds by Wes *et al.* [1] and Lehmberg *et al.* [2]. Its validity at high rotational speeds has still to be confirmed by experimental evidence.

With this assumption and taking into account the age distribution of the packets, relation (11) becomes

$$\Phi = \int_{S_w} K(\tau)(t_w - t_m)\,\mathrm{d}S(\tau) = \bar{K}(\tau_c)(t_w - t_m)S_w \quad (13)$$

with

$$\bar{K}(\tau_c) = (1/\tau_c)\int_0^{\tau_c} K(\tau)\,\mathrm{d}\tau = K_w. \quad (14)$$

The contact heat transfer coefficient between the load and the wall is then equal to the mean coefficient during the contact time, due to the transient conduction between the wall and a semi-infinite bed of particles.

Thermal contact resistance model

The transient wall–particle conduction heat transfer has been dealt with in numerous works. The existing models were recently discussed by Kubie [16].

The most widely used approach [2, 11, 13, 14, 17, 18] consists in considering the bed as a homogeneous solid, the physical properties of which are uniform and equal to the apparent properties of the material. To account for the increased voidage at the wall, a thermal contact resistance $1/K_c$, independent of time, is introduced at the wall–bed interface.

In this case, the time-mean Nusselt number can be approximated by the following analytical expression:

$$\overline{Nu} = 1/(1/Nu_c + (\lambda_g/\lambda_0)\sqrt{(\pi Fo)/2}). \quad (15)$$

The experimental coefficients have been correlated by means of this relation. Figures 7–9 compare the measured and calculated values; for each series of results, the contact Nusselt number Nu_c was adjusted to best fit the data. The fitting is fairly good: most experimental values fall within $\pm 10\%$ of the calculated ones. Some systematic discrepancies are observed for Fourier values smaller than 0.1.

At this point, we are able to discuss the assumption of complete mixing in the cascade. In order to verify that thermal mixing does not limit the heat transfer even at high rotational speeds, we will compare the contact Nusselt numbers obtained from our experiments with those measured in situations which do not involve any mixing at all: for instance, results obtained in moving beds by Ernst [13], Sullivan and Sabersky [17], and Botterill and Hampshire [19]; transient tests conducted by Gloski *et al.* [18] on fixed beds of particles will also be used.

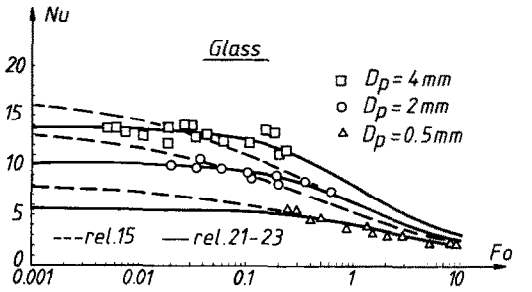

FIG. 7. Correlation of the measured Nusselt values—glass.

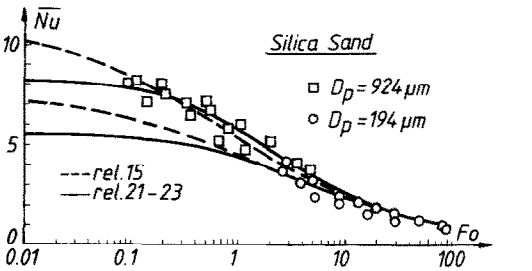

FIG. 8. Correlation of the measured Nusselt values—silica sand.

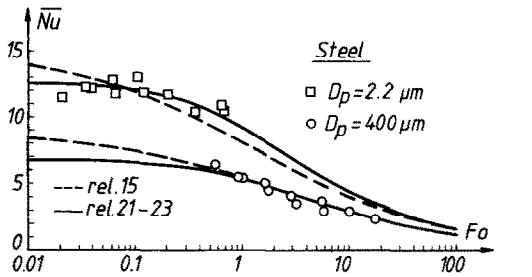

FIG. 9. Correlation of the measured Nusselt values—steel.

The most widely used approach [2, 11, 13, 14, 17, 18] consists in considering the bed as a homogeneous solid, the physical properties of which are uniform and equal to the apparent properties of the material. To account for the increased voidage at the wall, a thermal contact resistance $1/K_c$, independent of time, is introduced at the wall–bed interface.

In this case, the time-mean Nusselt number can be approximated by the following analytical expression:

$$\overline{Nu} = 1/(1/Nu_c + (\lambda_g/\lambda_0)\sqrt{(\pi Fo)/2}). \quad (15)$$

The experimental coefficients have been correlated by means of this relation. Figures 7–9 compare the measured and calculated values; for each series of results, the contact Nusselt number Nu_c was adjusted to best fit the data. The fitting is fairly good: most experimental values fall within $\pm 10\%$ of the calculated ones. Some systematic discrepancies are observed for Fourier values smaller than 0.1.

At this point, we are able to discuss the assumption of complete mixing in the cascade. In order to verify that thermal mixing does not limit the heat transfer even at high rotational speeds, we will compare the contact Nusselt numbers obtained from our experiments with those measured in situations which do not involve any mixing at all: for instance, results obtained in moving beds by Ernst [13], Sullivan and Sabersky [17], and Botterill and Hampshire [19]; transient tests conducted by Gloski *et al.* [18] on fixed beds of particles will also be used.

The contact Nusselt numbers determined by these authors are plotted in Fig. 10 together with our rotary drum values. Although widely dispersed, the different values have the same order of magnitude. The rotating cylinder data fall within the range of the values measured by the other techniques and show a similar trend of variation with particle diameter. Hence, the assumption of complete mixing seems adequate.

Contact resistance plus capacity model

Relation (15) does not fit very well the experimental coefficients for low Fourier values. This can be observed by inspecting the data obtained with large particle diameters (glass beads, 2 and 4 mm; steel shot, 2.2 mm). For $Fo < 0.1$, curve (15) deviates significantly from the experimental points.

It is due to the fact that, for such low Fourier numbers, heat does not penetrate the bed beyond the first layer of particles so that the material can no longer be considered as homogeneous. It appears

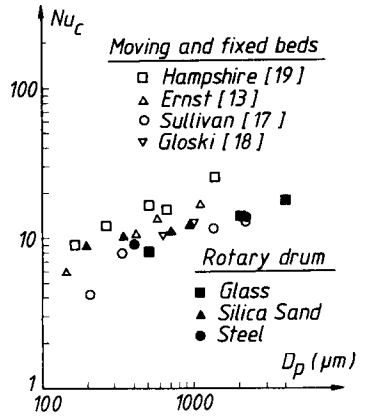

FIG. 10. Comparison of the contact Nusselt numbers calculated from equation (15) with literature data obtained in moving and fixed beds.

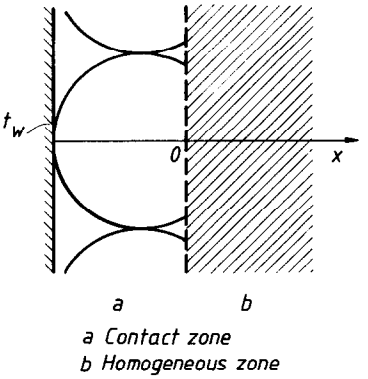

FIG. 11. Contact resistance plus capacity model—model geometry.

necessary to take into account separately the transient behaviour of the solid and the gaseous phases. A possible approach would be to use a 'discrete particle' model, first developed by Botterill and Williams [10], but this kind of model is limited to short contact times.

To our purpose, we have preferred to derive an analytical expression, valid in the whole range of Fourier number, by modifying the contact resistance model.

(1) The bed is divided into two zones (Fig. 11): (a) a 'contact zone', where the heterogeneity of the material is taken into account; this zone is constituted by discrete particles in contact with the wall; (b) a 'homogeneous zone', adjacent to the previous one, that has uniform properties, equal to the apparent properties of the material.

(2) In the contact zone, the temperature gradients inside the particles and the heat capacity of the gas phase are neglected. The solid phase of this zone acts as a 'contact capacity' exchanging with the wall through a constant contact resistance.

(3) The depth of the contact zone is about $0{\cdot}75D_p$. The selection of this value is based on the porosity profile measured by Benenati and Brosilow [20]. This depth corresponds to the point where the local void fraction is equal to the apparent porosity of the material, about 40%. The contact capacity can then be calculated as

$$C_c = \rho_s \cdot c_s \cdot (\text{number of particles per unit area}) \cdot (\text{volume of a particle between 0 and } 0.75D_p)$$

$$C_c = \frac{\rho_0 c_0}{1-\varepsilon_0}\frac{4a}{\pi D_p^2}\left(0.84375\frac{\pi D_p^3}{6}\right)$$

$$C_c = 0.84375\frac{2a}{3(1-\varepsilon_0)}\rho_0 c_0 D_p. \quad (16)$$

In equations (16), a is the 'surface coverage factor' i.e. the projected area of the first layer of particles divided by the area of the wall. From ref. [20], a value of 0.77 is taken for a.

With these assumptions, the temperature profile $t(x,\tau)$ in the homogeneous zone is given by

$$\rho_0 c_0 \frac{\partial t}{\partial \tau} = \lambda_0 \frac{\partial^2 t}{\partial x^2} \quad (17)$$

with initial condition

$$t(x,0) = t_m \quad (18)$$

and boundary conditions

$$-\lambda_0 \left.\frac{\partial t}{\partial x}\right|_{x=0} = K_c[t_w - t(0,\tau)] - C_c\frac{\partial t(0,\tau)}{\partial t} \quad (19)$$

$$\left.\frac{\partial t}{\partial x}\right|_{x=\infty} = 0. \quad (20)$$

The solution of equations (17)–(20) gives a complicated expression for the time-mean Nusselt number. But, by consideration of a combination of impedances, the mean transfer coefficient can be approximated by the following relation:

$$1/\overline{Nu} = [1/Nu_c + 1/\overline{Nu}_0]\Big/\left[1+\frac{Nu_c}{\overline{Nu}_0}\frac{1}{f_c(Fo)} \times (1-\exp(-f_c(Fo)))\right] \quad (21)$$

with

$$f_c(Fo) = 1.778\frac{(1-\varepsilon_0)}{a}\left[\frac{\lambda_g}{\lambda_0}Nu_c Fo + \frac{2}{\sqrt{\pi}}\sqrt{Fo}\right] \quad (22)$$

and

$$\overline{Nu}_0 = 2\lambda_0/(\lambda_g\sqrt{(\pi Fo)}). \quad (23)$$

Constant values are adopted for a and ε_0, respectively 0.77 and 0.4. The derivation of these relations can be found in the Appendix.

The measured Nusselt numbers have been correlated by equations (21)–(23), Nu_c remaining as a parameter adjusted for each series of data. These correlations are represented in Figs. 7–9. It clearly demonstrates that, over the whole range of Fourier num-

Table 3. Contact Nusselt numbers, resulting from equations (21)–(23)

Material	D_p (μm)	Nu_c
Glass	500	6.619
	2000	10.18
	4000	13.73
Silica sand	194	5.564
	343	6.850
	709	7.828
	924	8.251
Steel	400	6.765
	2200	12.67

bers, equations (21)–(23) fit the experimental values better than equation (15), with deviations smaller than 10% for most points.

Correlation of the contact Nusselt numbers

The contact Nusselt numbers, calculated from equations (21)–(23), are listed in Table 3. These values range from 5.5 to 14 and strongly depend on the particle diameters.

The concept of contact resistance and its physical meaning have been discussed by many authors. It is generally accepted that this resistance is related to the conduction heat transfer through the fluid between the wall and the particles directly adjacent to it.

The effect of the particle roughness on the contact Nusselt number can be approximated by equation (24), first derived by Ernst [13], which accounts for the steady heat conduction through the fluid, between the wall and a layer of particles that do not touch it: the contact Nusselt number is then given by

$$Nu_c = 4a\left[\left(\frac{2\delta}{D_p}+1\right)\ln\left(\frac{D_p}{2\delta}+1\right)-1\right] + (1-a)\frac{D_p}{D_p/2+\delta} \quad (24)$$

with δ being the distance between the wall and the particles, i.e. something of the order of the roughness height.

As shown by Schlunder [21], this relation remains valid for perfectly smooth contacting surfaces. In this case, the distance is related to the mean free path of the gas molecules and accounts for a reduced thermal conductivity in the vicinity of the contact points, where the distances between the surfaces are of the same order of magnitude as the mean free path (Smoluchowsky effect).

As shown on Fig. 12, the values in Table 3 can be correlated by equation (24), with values of δ ranging from 5 to 20 μm, values that are consistent with the roughness of common material. The average value of δ is 12 μm; with these values—calculated by regression using all the results—the differences between the measured Nu_c values and those computed by equation (24) are smaller than 25%.

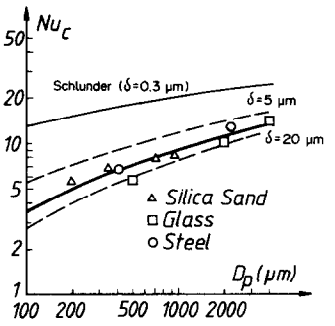

FIG. 12. Correlation of the contact Nusselt numbers calculated from equations (21)–(23) by the Ernst relation (equation (24)).

CONCLUSIONS

The wall–particles heat transfer has been investigated in batch fed horizontal cylinders, the internal wall of which was fitted out with longitudinal strips. Heat transfer coefficients were determined for nine particle diameters (from 194 μm to 4 mm). The influences of rotational speed (1–40 rev min^{-1}), filling degree (4–17%) and drum diameter (0.25 and 0.485 m) were investigated.

Starting from the observed transverse movement of the material, the heat transfer mechanism has been analysed. Two basic steps are involved: the transient conduction in the particle bed during its contact with the wall and the thermal mixing of hot and cold particles when they roll down the slope of the load. This mechanism can be described by a penetration model in which complete mixing is assumed. This assumption has been shown to be valid by comparing the coefficients measured in rotary drums with literature data obtained in moving and fixed beds, where no mixing limitations occur.

The wall–particles transient conduction can be modelled by a 'contact resistance plus capacity model', that takes into account the transient behaviour of the solid and the gaseous phases in the first layer of particles. Approximate analytical expressions, equations (21)–(23), have been derived, that relates the Nusselt number to the Fourier number.

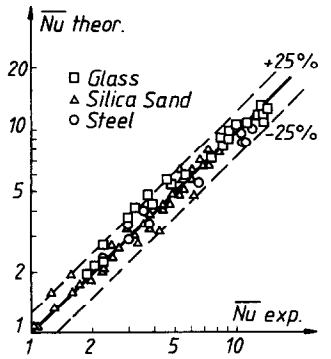

FIG. 13. Comparison of the experimental values with the values calculated by equations (21)–(24) (wall–particles distance δ = 12.6 μm).

By correlating the experimental data with the aid of these equations, the contact resistance value has been obtained for each tested material. The corresponding contact Nusselt numbers strongly depend on particle diameter and can be correlated by the Ernst equation (24), with an average wall–particles distance of about 12 μm. This distance is the only empirical parameter used to fit the experimental coefficients. The validity of the correlations derived in this work is shown on Fig. 13: most of the experimental values fall within 25% of the calculated ones.

REFERENCES

1. G. W. J. Wes, A. A. H. Drinkenburg and S. Stemerding, Heat transfer in a horizontal rotary drum reactor, *Powder Technol.* **13,** 185–192 (1976).
2. J. Lehmberg, M. Hehl and K. Schugerl, Transverse mixing and heat transfer in horizontal rotary drums reactors, *Powder Technol.* **18,** 149–163 (1977).
3. P. Lybaert, Contribution à l'étude du transfert de chaleur entre un matériau particulaire et la paroi dans les échangeurs rotatifs indirects, Thèse de Doctorat, Faculté Polytechnique de Mons (1985).
4. G. R. Reuter, Das Transport- und Mischverhalten von Drehrohröfenmöller bei der Erzeugung von Eisenschwamm, Doctorate Thesis, Technische Hochschule Aachen (1975).
5. M. Cross, The transverse motion of solids moving through rotary kilns, *Powder Technol.* **22,** 187–190 (1979).
6. H. E. Rose and R. M. E. Sullivan, *A Treatise on the Internal Mechanics of Ball, Tube and Rod Mills.* Constable, London (1958).
7. R. Rutgers, Longitudinal mixing of granular material flowing through a rotary cylinder—1. Descriptive and theoretical, *Chem. Engng Sci.* **20,** 1079–1087 (1965).
8. S. S. Wiedenbaum, Mixing of solids. In *Advances in Chemical Engineering,* Vol. 2, pp. 209–324. Academic Press, New York (1958).
9. J. Wunschman and E. U. Schlunder, Wärmeübergang von beheizten Flachen an Kugelschüttungen, *Verfahrenstechnik* **9,** 505–505 (1975).
10. J. S. M. Botterill and J. R. Williams, The mechanisms of heat transfer to gas-fluidized beds, *Trans. Instn Chem. Engrs* **41,** 217–230 (1963).
11. E. U. Schlunder, Der Wärmeübergang an ruhende, bewegte und durchwirbelte Schüttschichten, *Verfahrenstechnik* **14,** 459–468 (1980).
12. J. Kubie and J. Broughton, A model of heat transfer in gas fluidized beds, *Int. J. Heat Mass Transfer* **18,** 289–299 (1975).
13. R. Ernst, Der Mechanismus der Wärmeübergangs an Wärmeaustauchern in Fliessbetten, Doctorate Thesis, Technische Hoschschule Aachen (1959).
14. N. I. Gelperin and V. G. Einstein, Heat transfer in fluidized beds. In *Fluidization* (Edited by J. F. Davidson and D. Harrison). Academic Press, London (1971).
15. D. Kunii and O. Levenspiel, *Fluidization Engineering.* Wiley, New York (1969).
16. J. Kubie, Heat transfer between gas fluidized beds and immersed surfaces, *Int. J. Heat Mass Transfer* **28,** 1345–1353 (1985).
17. W. N. Sullivan and R. H. Sabersky, Heat transfer to flowing granular media, *Int. J. Heat Mass Transfer* **18,** 97–106 (1975).
18. D. Gloski, L. Glicksman and N. Decker, Thermal resistance at a surface in contact with fluidized bed particles, *Int. J. Heat Mass Transfer* **27,** 599–610 (1984).
19. J. S. M. Botterill and L. N. Hampshire, The gap between surface and particles in relative motion, *Chem. Engng Sci.* **23,** 400–402 (1968).
20. R. F. Benenati and C. B. Brosilow, Void fraction distribution in beds of spheres, *A.I.Ch.E. Jl* **8,** 359–361 (1962).
21. E. U. Schlunder, Wärmeübergang am bewegte Kugelschüttungen bei Kurzfristigem Kontact, *Chemie-Ingr-Tech.* **43,** 651–654 (1971).

APPENDIX

The situation to be modelled is sketched in Fig. A1.

Heat flux conservation can be written as

$$K_c(t_w - t(0,\tau)) = C_c \frac{dt(0,\tau)}{d\tau} + K_2(\tau)(t(0,\tau) - t_m) \quad \text{(A1)}$$

where $K_2(\tau)$ is the heat transfer coefficient associated with the semi-infinite homogeneous zone.

By defining a non-dimensional temperature θ as

$$\theta(\tau) = \frac{t(0,\tau) - t_m}{t_w - t_m} \quad \text{(A2)}$$

equation (A1) becomes

$$\frac{d\theta}{d\tau} = \frac{K_c}{C_c} - \left(\frac{K_c + K_2}{C_c}\right)\theta \quad \text{(A3)}$$

with the initial condition given by

$$\theta(0) = 0. \quad \text{(A4)}$$

To simplify the integration of equation (A4), the coefficient K_2 is assumed to be constant during the contact time, being equal to the mean coefficient calculated for a homogeneous semi-infinite body in perfect contact with a wall.

The solution of equations (A3) and (A4), with a constant K_2, is given by

$$\theta(\tau) = \frac{K_c}{K_c + K_2}\left[1 - \exp\left(-\frac{K_c + K_2}{C_c}\tau\right)\right]. \quad \text{(A5)}$$

The time-mean heat transfer coefficient can be expressed as

$$\bar{K}(\tau) = \frac{1}{\tau}\int_0^\tau K_c(1-\theta)\,d\tau \quad \text{(A6)}$$

which, after integration, gives

$$\frac{\bar{K}(\tau)}{K_c} = 1 - \frac{K_c}{K_c + K_2}\left[1 + \frac{C_c}{K_c + K_2} \times \left[\exp\left(-\frac{K_c + K_2}{C_c}\tau\right) - 1\right]\right] \quad \text{(A7)}$$

The value of K_2

$$K_2 = \frac{2\lambda_0}{\sqrt{(\pi\alpha_0\tau)}} \quad \text{(A8)}$$

and the value of the capacity given by equation (16) are then introduced in equation (A7).

Defining f_c as

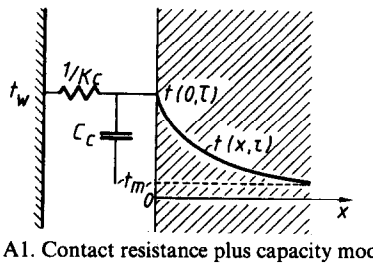

FIG. A1. Contact resistance plus capacity model.

$$f_c(Fo) = \frac{K_c + K_2}{C_c}\tau = \frac{3(1-\varepsilon_0)}{1.6875a} \times \left[\frac{K_c\tau}{\rho_0 c_0 D_p} + \frac{2\lambda_0\tau}{\rho_0 c_0 D_p\sqrt{(\pi a_0\tau)}}\right]$$

$$= \frac{3(1-\varepsilon_0)}{1.6875a}\left[\frac{\lambda_g}{\lambda_0} Nu_c Fo + \frac{2}{\sqrt{\pi}}\sqrt{Fo}\right] \quad \text{(A9)}$$

and rearranging the terms of equation (A7) yields equation (21).

TRANSFERT THERMIQUE PAROI-PARTICULES DANS LES ECHANGEURS ROTATIFS

Résumé—On a mesuré le coefficient de transfert de chaleur particules-paroi dans des échangeurs rotatifs de petites dimensions. Les essais ont été effectués avec neuf matériaux granulaires de natures différentes et de granulométries comprises entre 194 μm et 4 mm. On a étudié les effets de la vitesse de rotation (1–40 rev min^{-1}), du taux de remplissage (4–17%) et du diamètre du cylindre (0.25 et 0.485 m). Les valeurs expérimentales ont été corrélées à l'aide d'une relation approximative qui fait intervenir une résistance de contact à la paroi, la capacité calorifique des particules au voisinage de la paroi et la résistance à la pénétration de la chaleur au sein du lit de particules. On montre que la résistance de contact est due à la rugosité des particules. Une rugosité moyenne de 12 μm permet de rendre compte de manière satisfaisante des coefficients mesurés.

WÄRMEÜBERGANG ZWISCHEN WAND UND TEILCHEN IN ROTIERENDEN WÄRMETAUSCHERN

Zusammenfassung—Der Wärmeübergangskoeffizient zwischen Wand und Teilchen in kleinen Drehtrommelwärmetauschern wurde gemessen. Es wurden Experimente mit neun verschiedenen Granulaten durchgeführt, wobei der Teilchendurchmesser zwischen 194 μm und 4 mm lag. Die Einflüsse der Drehzahl (1–40 rev min^{-1}), des Füllgrades (4–17%) und des Trommeldurchmessers (0,25 und 0.485 m) wurden untersucht. Die experimentellen Daten wurden mit einer halbempirischen Beziehung korreliert, die den Kontaktwiderstand an der Wand, die Wärmekapazität der direkt an der Wand liegenden Teilchen und den Wärmeeindringwiderstand des Teilchenbettes beinhaltet. Der Kontaktwiderstand beruht auf der Rauhigkeit der Teilchen. Eine mittlere Rauhigkeitshöhe von 12 μm ergibt eine gute Übereinstimmung zu den gemessenen Wärmeübergangskoeffizienten.

ТЕПЛООБМЕН МЕЖДУ СТЕНКОЙ И ЧАСТИЦАМИ ВО ВРАЩАЮЩИХСЯ ТЕПЛООБМЕННИКАХ

Аннотация—Измерен коэффициент теплообмена между стенкой и частицами во вращающихся барботажных малогабаритных теплообменниках. Экспериментальные исследования проведены для девяти различных зернистых материалов с диаметром частиц от 194 мкм до 4 мм. Изучалось влияние скорости вращения (1–40 об/мин), степени заполнения (4–17%) и диаметра барабана (0,25 и 0,485 м). Проведено обобщение экспериментальных данных с помощью полуэмпирического соотношения, учитывающего контактное сопротивление у стенки, теплоемкость частиц в окрестности стенки и сопротивление теплопереносу в объеме слоя частиц. Показано, что контактное сопротивление определяется шероховатостью частиц. Найдено, что при средней высоте шероховатости, равной 12 мкм, наблюдается хорошее соответствие с результатами измерений.